



BRAIN DYNAMICS AT MULTIPLE SCALES: CAN ONE RECONCILE THE APPARENT LOW-DIMENSIONAL CHAOS OF MACROSCOPIC VARIABLES WITH THE SEEMINGLY STOCHASTIC BEHAVIOR OF SINGLE NEURONS?

SAMI EL BOUSTANI and ALAIN DESTEXHE
*Unité de Neurosciences Intégratives et Computationnelles (UNIC),
 CNRS, Gif-sur-Yvette, France*

Received November 12, 2008; Revised August 1, 2009

Nonlinear time series analyses have suggested that the human electroencephalogram (EEG) may share statistical and dynamical properties with chaotic systems. During slow-wave sleep or pathological states like epilepsy, correlation dimension measurements display low values, while in awake and attentive subjects, there is no such low dimensionality, and the EEG is more similar to a stochastic variable. We briefly review these results and contrast them with recordings in cat cerebral cortex, as well as with theoretical models. In awake or sleeping cats, recordings with microelectrodes inserted in cortex show that global variables such as local field potentials (local EEG) are similar to the human EEG. However, neuronal discharges are highly irregular and exponentially distributed, similar to Poisson stochastic processes. To reconcile these results, we investigate models of randomly-connected networks of integrate-and-fire neurons, and also contrast global (averaged) variables, with neuronal activity. The network displays different states, such as “synchronous regular” (SR) or “asynchronous irregular” (AI) states. In SR states, the global variables display coherent behavior with low dimensionality, while in AI states, the global activity is high-dimensionally chaotic with exponentially distributed neuronal discharges, similar to awake cats. Scale-dependent Lyapunov exponents and ϵ -entropies show that the seemingly stochastic nature at small scales (neurons) can coexist with more coherent behavior at larger scales (averages). Thus, we suggest that brain activity obeys a similar scheme, with seemingly stochastic dynamics at small scales (neurons), while large scales (EEG) display more coherent behavior or high-dimensional chaos.

Keywords: Electroencephalogram; correlation dimension; Lyapunov exponents; epsilon-entropy; network models.

1. Introduction

A number of methods from nonlinear dynamical systems have been applied to the different states of the human EEG. Early studies have calculated correlation dimensions from EEG and reported evidence for low-dimensional chaos in slow-wave sleep [Babloyantz *et al.*, 1985; Mayer-Kress *et al.*, 1988], as well as for pathological states such as epilepsy [Babloyantz & Destexhe, 1986; Frank *et al.*, 1990]

or the terminal state of Creutzfeldt–Jakob disease [Destexhe *et al.*, 1988]. These findings have been confirmed by numerous studies (reviewed in [Destexhe, 1992; Elbert *et al.*, 1994; Korn & Faure, 2003]). Interestingly, in these studies, the EEG dynamics during wakefulness or REM sleep did not show evidence for low-dimensional dynamics. These results were also corroborated with other measurements such as Lyapunov exponents, entropies,

power spectral densities, autocorrelations and symbolic dynamics [Destexhe, 1992].

The existence of low-dimensional chaotic dynamics in systems with such large degrees of freedom is surprising. Chaotic dynamics in extended coupled systems have been studied extensively for the last decades and is still a matter of intense investigation. In particular, for network of simplified neurons, as the spin-glass models, mean-field theories have proven the existence of stable chaotic attractors [Sompolinsky *et al.*, 1988; van Vreeswijk & Sompolinsky, 1996, 1998]. These systems have been shown to exhibit chaotic persistence regarding parameter changes [Albers *et al.*, 2006], a property that makes chaotic dynamics more common than exceptional [Spratt, 2008]. From a computational point of view, chaotic behavior or nearly chaotic regime (edge of chaos) can be optimal for information processing [Bertschinger & Natschläger, 2004; Legenstein & Maass, 2007]. In network models of spiking neurons, chaotic regimes have also been studied [Cessac, 2008; Cessac & Viéville, 2008] and can be present only as transients during which the system is numerically indistinguishable from a usual chaotic attractor. However the lifetime of these transient periods is known to increase exponentially with network size [Crutchfield & Kaneko, 1988; Tél & Lai, 2008] making them more relevant in practice than the real stable attractor for large enough networks.

In this paper, we intend to study a specific spiking neuron model which displays these properties and yield biophysical behavior relevant to understand EEG data. Classical nonlinear tools as the correlation dimension or the Lyapunov exponents have given some insight on macroscopic quantities as the EEG or the overall activity of numerical models but are often criticized because of their limitation for low-dimensional dynamics [Kantz & Schreiber, 2004]. In order to distinguish between microscopic dynamics and collective behavior, we borrow recent tools developed in the context of high-dimensional systems and which offer the analysis at different scales. In particular, finite-size Lyapunov exponent [Aurell *et al.*, 1997] as well as ϵ -entropy [Gaspard & Wang, 1993] provide a scale-dependent description of spiking neuron networks and could detect whether or not low-dimensional dynamics prevail at macroscopic scales. These tools will be applied to EEG data as well as numerical models.

2. Methods

In this section, we briefly describe the analytical and numerical tools which will be used to probe the nonlinear nature of the EEG recordings or the numerical simulations. Most of these analysis are extensively used in the literature. Furthermore, we used the TISEAN toolbox [Hegger *et al.*, 1999] to perform most of our nonlinear analysis. We also give information about the numerical model.

2.1. Phase space reconstruction

We have used the method of time-delayed vectors of the time series, which yields reconstructed attractors topologically equivalent to the original attractor of the system [Takens, 1981; Sauer *et al.*, 1991]. We chose a fixed delay parameter determined by the first minimum of the mutual information [Fraser & Swinney, 1986]. The embedding dimension was chosen such that any self-similar asymptotic behavior saturates beyond this dimension, indicating a successful attractor reconstruction.

2.2. Correlation dimension

The correlation dimension was measured from the correlation integral [Grassberger & Procaccia, 1983] which is estimated by using

$$C(\epsilon) = \frac{1}{N^2} \sum_{i,j=1}^N \Theta(\epsilon - \|\mathbf{x}(i) - \mathbf{x}(j)\|) \quad (1)$$

where $\mathbf{x}(i) \in \mathbb{R}$ is the m -dimensional delay vector and ϵ is a threshold distance which reflects the scale under consideration. Moreover we used a Theiler window [Theiler, 1990] according to the temporal correlation of each time series to avoid spurious estimation. If the correlation integral manifests a power-law behavior over a range of scale which saturates with increasing embedding dimension, the correlation dimension is simply the corresponding power-law coefficient.

2.3. Recurrence plots

This tool provides an intuitive visualization of recurrences in trajectories on the attractor [Eckmann *et al.*, 1987]. The recurrence matrix is defined by

$$RP(i, j) = \Theta(\epsilon - \|\mathbf{x}(i) - \mathbf{x}(j)\|) \quad (2)$$

where the matrix entry is equal to 1 if the trajectory \mathbf{x} at i is in the ϵ -neighbor of itself at j and 0 otherwise. Stereotypic patterns in the recurrence plot can indicate the existence of periodic behavior, low-dimensional chaos or stochastic-like dynamics. In particular, diagonal lines are typical of periodic dynamics whereas clouds of dots are produced by a stochastic component. For an extensive review on recurrence plot, the reader should refer to [Marwan *et al.*, 2006].

2.4. Finite-size Lyapunov and ϵ -entropy

Scale-dependent nonlinear analysis has been greatly studied the last decade and come in handy to distinguish deterministic (possibly chaotic) dynamics from stochastic noise. In this paper, we will mainly consider two quantities: the Finite-Size Lyapunov Exponent (FSLE) and ϵ -entropy. The former was introduced in the context of developed turbulence [Aurell *et al.*, 1997] and has proven to be more suited for a broad range of systems where the dynamics exhibit low-dimensional chaotic behavior only on large-scale [Shibata & Kaneko, 1998; Cencini *et al.*, 1999; Gao *et al.*, 2006]. Roughly, if we want to quantify the sensitivity to initial conditions on large scales, it is necessary to consider perturbations which are not infinitesimal. Therefore, the FSLE can be defined as follows

$$\lambda(\delta) = \frac{1}{\langle T_r(\delta) \rangle} \left\langle \ln \left(\frac{\Delta_r}{\delta} \right) \right\rangle \quad (3)$$

where for a perturbation between two initial trajectories δ , T_r is the minimal time required for those trajectories to be separated by a distance Δ_r greater than or equal to δr where $r = 2$ is usually taken. The brackets in Eq. (3) denote averages on the attractor for many realizations. The ϵ -entropy is a generalization of the Kolmogorov–Sinai entropy rate [Gaspard & Wang, 1993] which is defined for a finite scale ϵ and time delay τ by

$$h(\epsilon, \tau) = \lim_{m \rightarrow \infty} h_m(\epsilon, \tau) \quad (4)$$

$$= \frac{1}{\tau} \lim_{m \rightarrow \infty} \frac{1}{m} H_m(\epsilon, \tau) \quad (5)$$

with

$$h_m(\epsilon, \tau) = \frac{1}{\tau} (H_{m+1}(\epsilon, \tau) - H_m(\epsilon, \tau)) \quad (6)$$

where $H_m(\epsilon, \tau)$ is the entropy estimated with box partition of the phase space for box size given by ϵ on the attractor reconstructed with a time delay

τ and an embedding dimension m . This quantity exhibits a plateau on particular scales if a deterministic low-dimensional dynamics occurs at these scales. It can thus be used to describe large scale dynamics independently of the small scale noisy behavior or can be used to distinguish noise from chaos in some cases [Cencini, 2000].

2.5. Avalanche analysis

To identify the presence of scale invariance, typical of self-organized critical states [Jensen, 1998], we used an “avalanche analysis” methods [Beggs & Plenz, 2003]. This method consists of detecting “avalanches” as clusters of contiguous events separated by silences, by binning the system’s activity in time windows (1 ms to 16 ms were used). Cluster of events were defined from the spike times among the ensemble of simultaneously recorded neurons. The scale invariance was determined from the distribution of avalanche size, calculated as the total number of events [Beggs & Plenz, 2005].

2.6. Network of integrate-and-fire neurons

Networks of “integrate-and-fire” neurons were simulated according to models and parameters published previously [Vogels & Abbott, 2005; El Boustani *et al.*, 2007]. The network consisted of 5000 neurons, which were separated into two populations of excitatory and inhibitory neurons, forming 80% and 20% of the neurons, respectively. All neurons were connected randomly using a connection probability of 2%.

The membrane equation of cell i was given by:

$$C_m \frac{dV_i}{dt} = -g_L(V_i - E_L) + S_i(t) + G_i(t), \quad (7)$$

where $C_m = 1 \mu\text{F}/\text{cm}^2$ is the specific capacitance, V_i is the membrane potential, $g_L = 5 \times 10^{-5} \text{S}/\text{cm}^2$ is the leak conductance density and $E_L = -60 \text{mV}$ is the leak reversal potential. Together with a cell area of $20\,000 \mu\text{m}^2$, these parameters give a resting membrane time constant of 20 ms and an input resistance at rest of $100 \text{M}\Omega$. The function $S_i(t)$ represents the spiking mechanism intrinsic to cell i and $G_i(t)$ stands for the total synaptic current of cell i . Note that in this model, excitatory and inhibitory neurons have the same properties.

In addition to passive membrane properties, IF neurons had a firing threshold of -50mV . Once the V_m reaches threshold, a spike is emitted and

the membrane potential is reset to -60 mV and remains at that value for a refractory period of 5 ms. This model was inspired from a previous publication reporting self-sustained irregular states [Vogels & Abbott, 2005].

Synaptic interactions were conductance-based, according to the following equation for neuron i :

$$G_i(t) = - \sum_j g_{ji}(t)(V_i - E_j), \quad (8)$$

where V_i is the membrane potential of neuron i , $g_{ji}(t)$ is the synaptic conductance of the synapse connecting neuron j to neuron i , and E_j is the reversal potential of that synapse. E_j was 0 mV for excitatory synapses, or -80 mV for inhibitory synapses.

Synaptic interactions were implemented as follows: when a spike occurred in neuron j , the synaptic conductance g_{ji} was instantaneously incremented by a quantum value ($q_e = 6$ nS and $q_i = 67$ nS for excitatory and inhibitory synapses, respectively) and decayed exponentially with a time constant of $\tau_e = 5$ ms and $\tau_i = 10$ ms for excitation and inhibition, respectively.

3. Evidence for Chaotic Dynamics in EEG Activity

Human EEG recordings during different brain states are illustrated in Fig. 1, along with a two-dimensional representation of the phase portrait obtained from each signal. During wakefulness (eyes open) and REM sleep, the dynamics is characterized by low-amplitude and very irregular EEG activity, while during deep sleep, the EEG displays slow waves (“delta waves”) of large amplitude. Oscillatory dynamics with a frequency around 10 Hz is seen in the occipital region when the eyes are closed (“alpha rhythm”). Pathological states, such as epilepsy or comatous states, display large amplitude oscillations, which are strikingly regular.

A first evidence for chaotic dynamics is that EEG dynamics display a prominent sensitivity to initial conditions. This sensitivity is illustrated in Fig. 2 for the alpha rhythm (awake eyes closed) and slow-wave sleep (stage IV). A set of close initial conditions is defined by choosing neighboring points in phase space, and this set of points is followed in time. The divergence of the trajectories emanating from each initial condition is evident from the illustration in Fig. 2, and is actually exponential. This exponential divergence betrays the presence of at least one positive Lyapunov exponent. A more

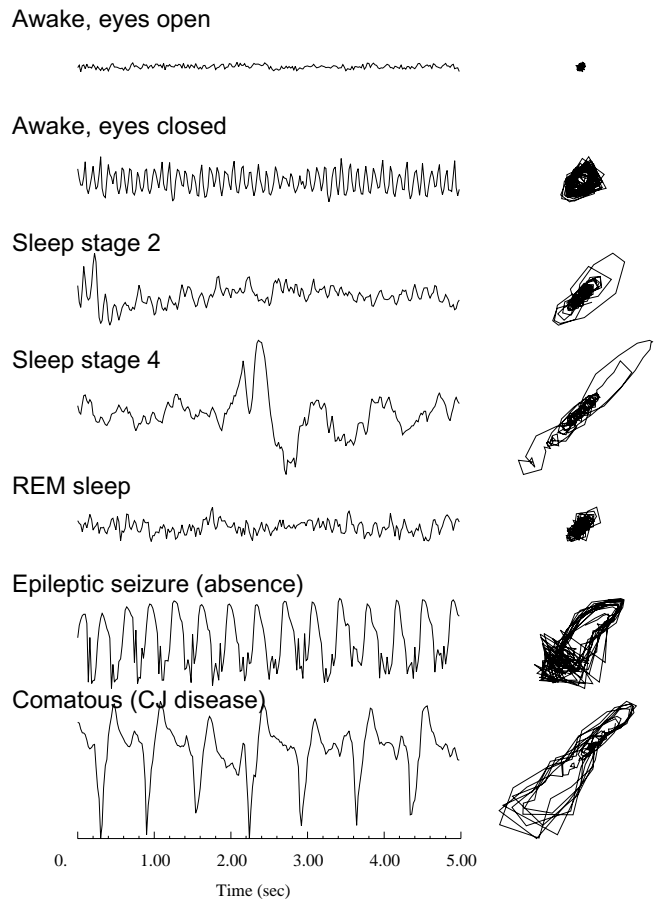


Fig. 1. Electroencephalogram signals and phase portraits during different brain states in humans. (Left) 5 seconds of EEG activity in different brain states (same amplitude scale). (Right) 2-dim phase portrait of each signal. Modified from [Destexhe, 1992].

quantitative investigation using numerical methods [Wolf *et al.*, 1985] reveals the presence of positive Lyapunov exponents for all EEG states investigated [Destexhe, 1992].

EEG dynamics also displays other characteristics of chaotic dynamical systems, such as broad-band power spectra (not shown) and fractal attractor dimensions. This latter point was investigated by a number of laboratories, and is summarized in Fig. 3. Correlation integrals $C(r)$ are calculated from the reconstructed phase portraits for different embedding dimensions [Figs. 3(a) and 3(b)]. The correlation dimension d is obtained by estimating the scaling of $C(r)$ by using logarithmic representations, in which the slope directly gives an estimate of d . The calculation of d as a function of the embedding dimension Fig. 3(c) saturates to a constant value for some states (such as deep sleep or pathologies), but not for others. This is the case

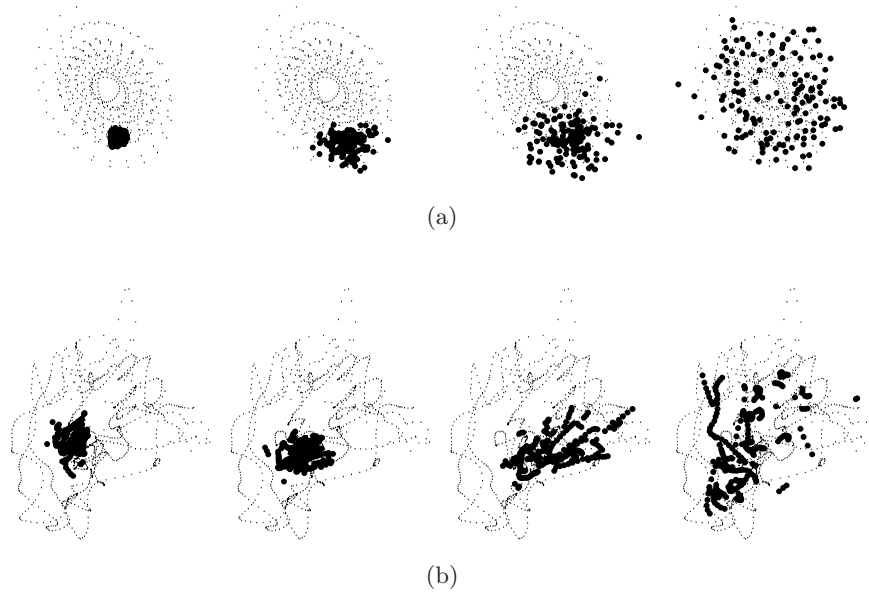


Fig. 2. Illustration of the sensitivity to initial conditions in EEG dynamics. A cluster of neighboring points in phase space (leftmost panels) is followed in time and is shown on the same phase portrait after 200 ms, 400 ms and 3 s (from left to right; same data as in Fig. 1). (a) Awake eyes closed; (b) Sleep stage IV. Modified from [Destexhe, 1992].

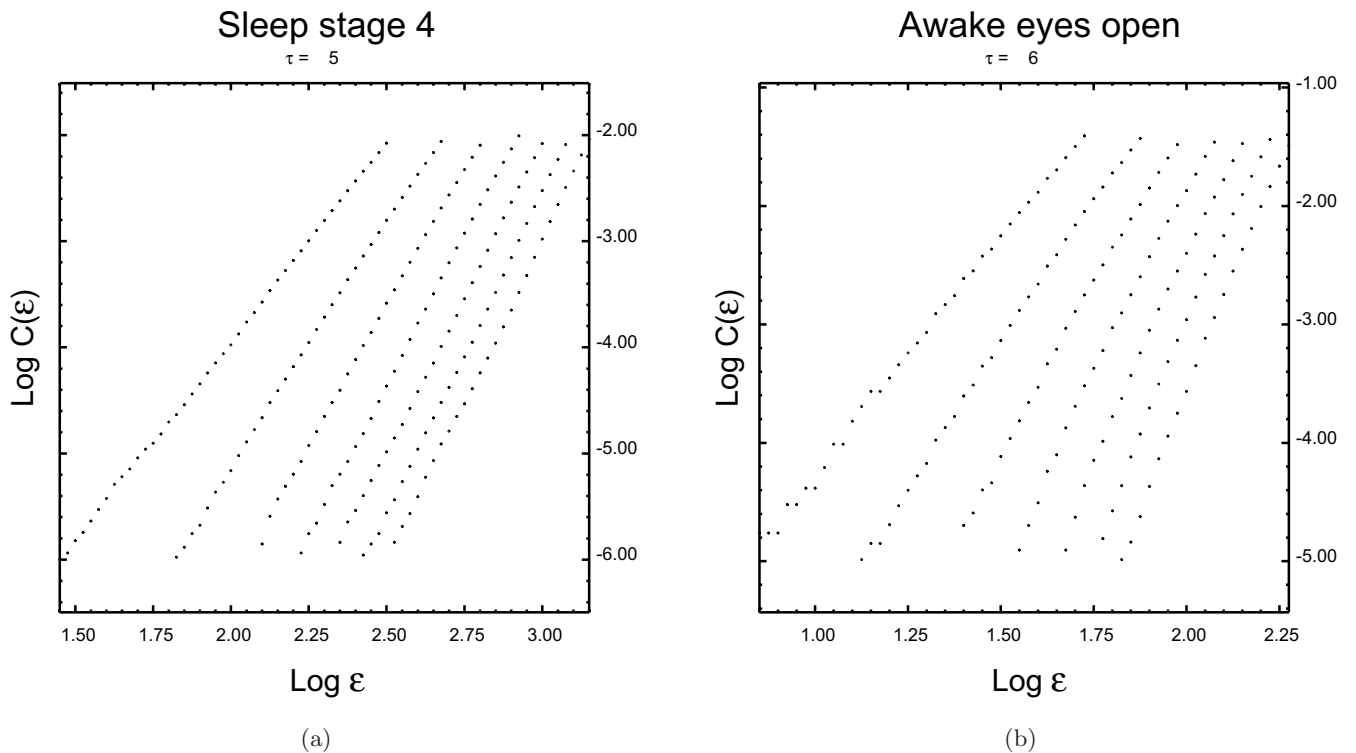
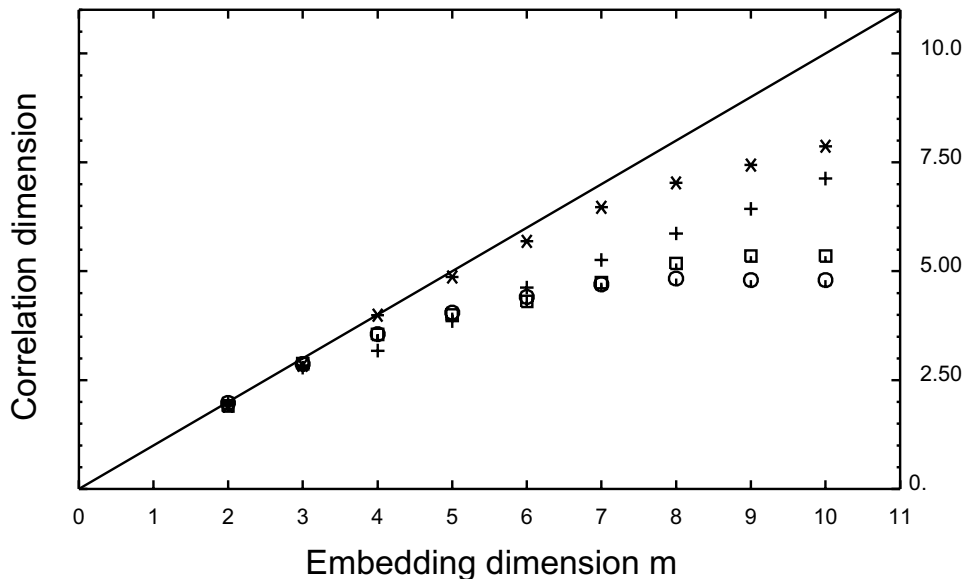


Fig. 3. Correlation dimension calculated from different brain states in humans. (a) Correlation integrals $C(r)$ calculated from sleep stage IV. (b) Correlation integrals calculated from Awake eyes open. (c) Correlation dimension as a function of embedding dimension for different brain states. Symbols: * = Awake eyes open, + = REM sleep, squares = sleep stage 2, circles = sleep stage 4. Modified from [Destexhe, 1992].



(b)

Fig. 3. (Continued)

for the EEG during wakefulness, which dimension d does not saturate, which is a sign of high dimensionality.

The correlation dimensions obtained for different brain states are represented in Fig. 4 as a function of the mean amplitude of the EEG signal. This representation reveals a “hierarchy” of dimensionalities for the EEG. The aroused states, such as wakefulness and REM sleep, are characterized by high dimension and no sign of slow-wave activity. As the brain drifts towards sleep, the dimensionality

decreases and attains its lowest level during the deepest phase of sleep, in which the EEG is dominated by large-amplitude slow waves. A further decrease is seen during pathologies, which are also dominated by slow-wave activity.

4. Evidence for Stochastic Dynamics in Brain Activity

The above results are consistent with the idea that awake brain activity may be associated with high-dimensional dynamics, perhaps analogous to a stochastic system. To further investigate this aspect, we have examined data from animal experiments in which both microscopic (cells) and macroscopic (EEG) activities can be recorded. The correspondence between these variables is shown in Fig. 5 for cat cerebral cortex during wakefulness and slow-wave sleep.

Those electrical measurements were made using tungsten microelectrodes directly inserted in cortical gray matter [Destexhe *et al.*, 1999]. This recording system enables the extraction of two signals: a global signal, similar to the EEG, which is called “local field potential” (LFP) and reflects the averaged electrical activity of a large population of neurons. In addition, single neurons can be distinguished and can be extracted. These signals are shown and compared in Fig. 5. During wakefulness, the LFP shows low-amplitude irregular activity, while neuronal discharges seem random. Slow-wave

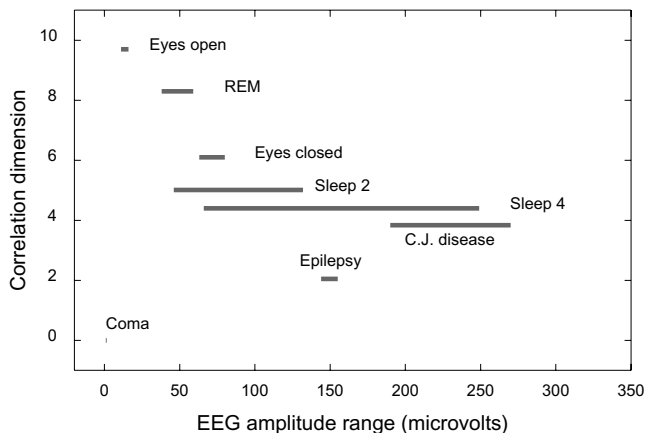


Fig. 4. Dimension — amplitude representation for different brain states. The correlation dimension of the EEG is shown as a function of the amplitude range (maximal amplitude deflection calculated over 1 s periods. Modified from [Destexhe, 1992].

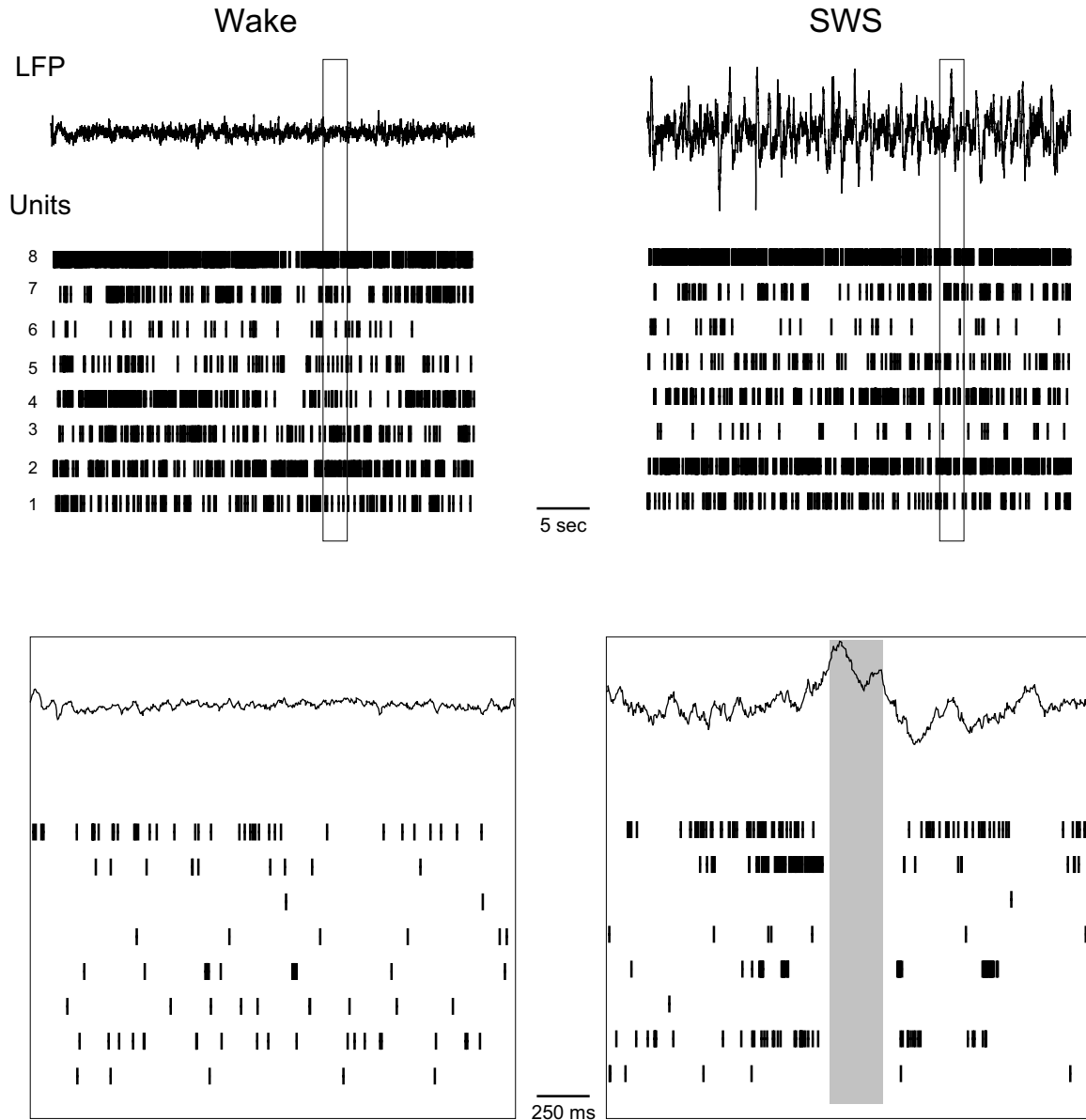


Fig. 5. Distributed firing activity and local field potentials in cat cortex during wake and sleep states. Recordings were done using eight bipolar tungsten electrodes in cat parietal cortex (data from [Destexhe *et al.*, 1999]). The irregular firing activity of eight multi-units is shown at the same time as the LFP recorded in electrode 1. During wakefulness, the activity is sustained and irregular (see magnification below). During slow-wave sleep (SWS), the activity is similar as wakefulness, except that “pauses” of firing occur in all cells, and in relation to the slow waves (one example is shown in gray in the bottom graph). The boxes in the top graphs are shown in bottom graphs at 20 times higher temporal resolution.

sleep is characterized by dominant delta waves in the LFP, as in human sleep stage IV. The occurrence of slow waves is correlated with a concerted pause in the firing of the neurons [Destexhe *et al.*, 1999].

Analyzing the spike discharge of single neurons revealed that the interspike-intervals (ISI) are exponentially distributed, in a manner indistinguishable from a Poisson stochastic process [Fig. 6(a)]. Performing an avalanche analysis revealed that the

distribution of avalanche size from the neuronal discharges was also exponential [Fig. 6(b)]. The same scaling could be explained by uncorrelated Poisson processes, as if the neurons discharged randomly and independently. This analysis was reproduced from a previous study [Bedard *et al.*, 2006].

Thus, these data and analysis show that the dynamics of neuronal activity in the awake cerebral cortex is similar to stochastic processes. The statistics of the ISI distributions, as well as the collective

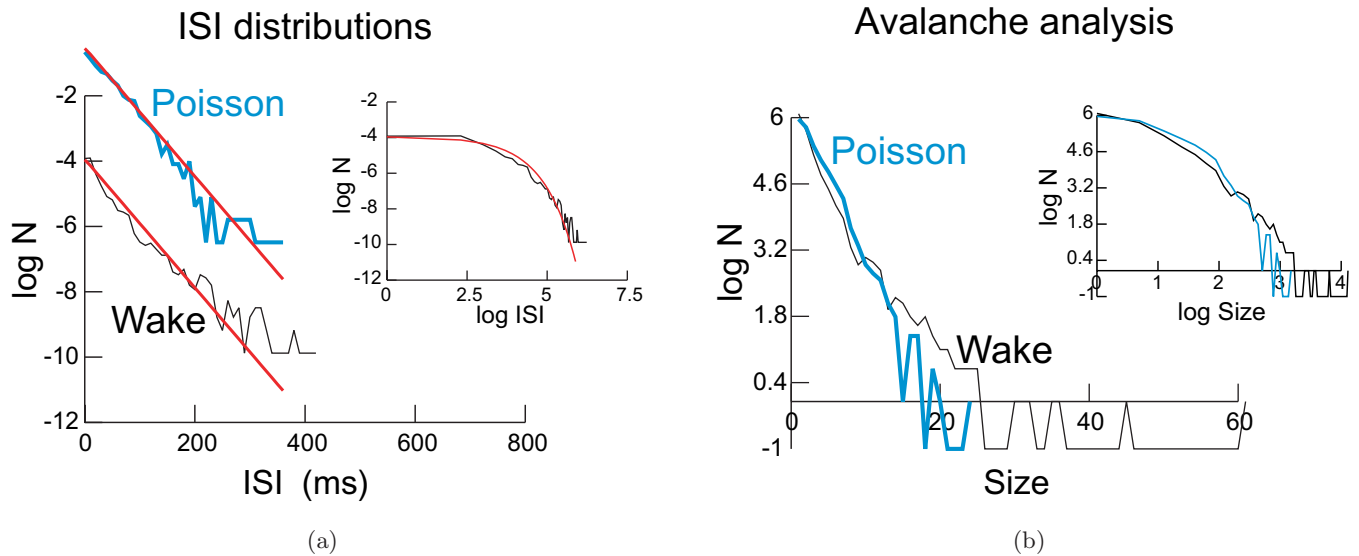


Fig. 6. Analysis of neuronal activity in awake cat cerebral cortex. (a) Interspike interval (ISI) distributions computed from extracellularly recorded neurons in wakefulness (natural logarithms). A Poisson process with the same average rate is shown for comparison (blue; curve displaced upwards for clarity). The inset shows a log–log representation. The red curves indicate the theoretical value for Poisson processes. (b) Avalanche analysis of extracellular recordings in the awake cat (natural logarithms). The same analysis was performed on surrogate data (blue; Poisson processes). The inset shows the same data in log–log representation. Modified from [Bedard *et al.*, 2006].

dynamics (“avalanches”) cannot be distinguished from a Poisson stochastic process.

5. Models of Irregular Dynamics in Neuronal Networks

We next consider if this type of dynamics can be found in theoretical models of neuronal networks. We consider randomly-connected networks of excitatory and inhibitory point neurons, in which firing activity is described by the “integrate-and-fire” model, while synaptic interactions are conductance-based. As shown in previous publications [Vogels & Abbott, 2005; El Boustani *et al.*, 2007], this model can display states of activity consistent with recordings in awake neocortex, as shown in Fig. 7. The network can display different types of states, such as “synchronous regular” (SR) states, or “asynchronous irregular” (AI), both of which are illustrated in Fig. 7. In SR states, the activity is oscillatory and synchronized between neurons, while in AI states, neurons are desynchronized and fire irregularly, similar to recordings in awake cats (compare with cells in Fig. 5). The averaged activity of the network is coherent and of high amplitude in SR states, but is very noisy and of low amplitude in AI states, similar to the EEG or LFP activity seen in wakefulness (compare with EEGs in Fig. 1 and LFPs in Fig. 5).

The time series of these averaged network activities (bottom graphs in Fig. 7) were analyzed similarly to the EEG in Sec. 3. We were particularly interested in the transition region between AI and SR states where the firing loses its coherence. This trajectory in the phase diagram is shown as a black rectangle in the upper panels of Fig. 7 and is characterized by an abrupt drop of activity concomitant with an increasing irregular firing. Similar results can be obtained by reducing the excitatory synaptic strength instead. However, to avoid a loss of stability, we preferred to study the transition by increasing the inhibitory synaptic strength. Phase portraits of SR and AI states, as well as the corresponding recurrence plots, are illustrated in Fig. 8. As expected, SR states (leftmost panel in Fig. 8) display a limit cycle phase portrait, while AI states (rightmost panel) appear as a dense unstructured attractor. When the dynamics is dominated by inhibition the limit cycle is rapidly blurred by small-scale fluctuations which become ubiquitous for AI states. However, even though the phase portrait does not display any structure, the recurrence plot still exhibits a strong deterministic component (diagonal line) which is completely lost for a state well beyond the boundary region (noisy recurrence plot).

To quantify this progressive release of degree of freedom, we estimated the correlation dimension

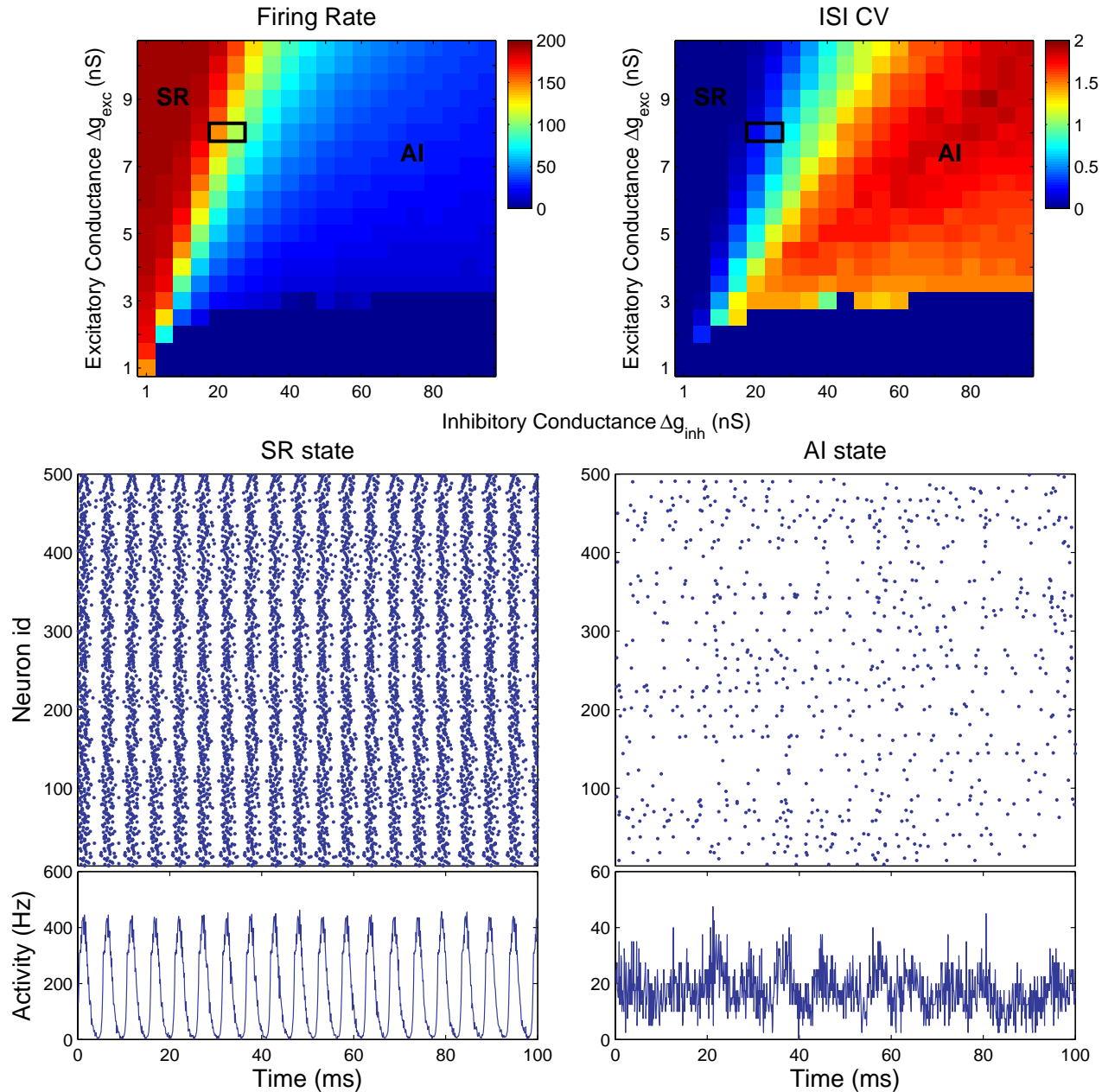


Fig. 7. Different network states in randomly-connected networks of spiking neurons. (Top) State diagrams representing the average firing rate (left) and the firing irregularity (ISI CV, right) of a randomly-connected network of 5000 integrate-and-fire neurons with a sparse connectivity of 2%. The phase diagram is drawn according to the excitatory and inhibitory quantal conductance. For increasing inhibition the dynamics undergo a transition from synchronous firing among the neuron and regular firing to a state where the synchrony has substantially decreased and neurons fire irregularly. The black rectangle indicates a transition from the SR to the AI regime. We selected this region for the rest of the study (see next figures). (Bottom) The two different states, “Synchronous Regular” (SR, left) and “Asynchronous Irregular” (AI, right). The corresponding regions in the state diagram are indicated on top. For both panels, the upper part shows a raster plot of 500 neurons taken randomly from the network. Each dot is a spike emitted by the corresponding neuron across time. In the lower part, the mean firing rate is computed among the whole network with a time bin of 0.1 ms. The asynchronous activity is reflected through the less fluctuating mean activity.

on the overall activity for those different states. Figure 9 shows the computed dimension for three different embedding dimensions. The network activity displays a low-dimension dynamics as expected

for SR state whereas the dimension suddenly increases with increasing inhibition conductance. Moreover, the corresponding values do not saturate with increasing embedding dimension suggesting a

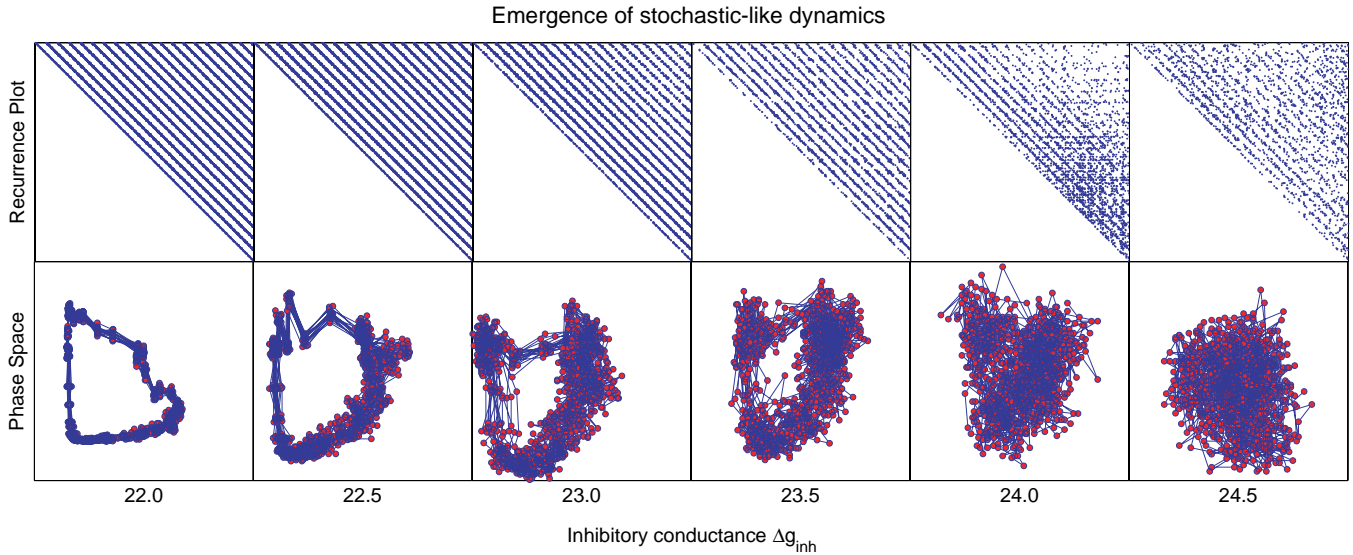


Fig. 8. Recurrence plot and phase portraits of different network states. From left to right, different step of the transition from the SR state (leftmost) to AI state (rightmost). All states differed by the value of the inhibitory conductance Δg_{inh} , as indicated. The top graphs indicate the recurrence plot. The diagonals indicate the existence of a dominant periodic component. As the slaved degrees of freedom are unleashed with increasing inhibition, the recurrence plot is blurred by the stochastic-like component emerging at larger scales. This is the manifestation of the transition to a high-dimensional dynamics. For network states in the middle of the AI region, there is almost no visible recurrency and the recurrence plot looks like that of a stochastic process. The bottom graphs show bi-dimensional phase space reconstruction of the corresponding state. We can clearly see the “noisy” limit cycle which progressively degenerates into a dense high-dimensional attractor confirming what is shown by the recurrence plot.

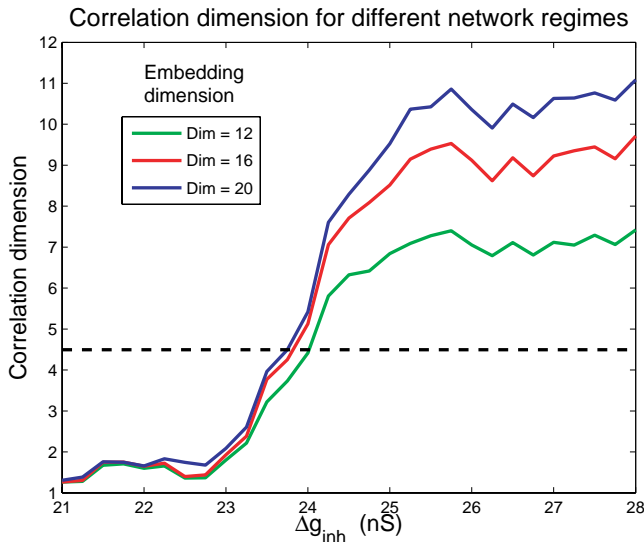


Fig. 9. Transition to a high-dimensional attractor in the AI regime. The correlation dimension is plotted according to the network state from the SR to the AI regime. Saturation of the scaling region in the correlation integral is shown by illustrating the estimated correlation dimension for three embedding dimensions. Below the dotted line, the measure is considered to saturate correctly whereas above this line, the measure cannot be trusted anymore. In particular, for low inhibition conductances, there are severe shifts with increasing embedding dimension. The dotted line is given by the disappearance of the plateau in the ϵ -entropy of Fig. 12.

high-dimensional attractor. Therefore, beyond the dotted black line, the correlation dimension is not a relevant measure anymore.

We also analyzed the spiking activity of the model using the same statistical tools as for experimental data. The distribution of ISIs during AI states was largely dominated by an exponential component [Fig. 10(a)], very similar to experimental data [compare with Fig. 6(a)]. Analyzing population activity, through “avalanche analysis”, displayed exponential distributions [Fig. 10(b)], also similar to experimental data [compare with Fig. 6(b)]. Power-law scaling was also present for a limited range (see Fig. 10(b), inset). Similar results were obtained for different network states (not shown).

One can ask what would be the effect of a more specific connectivity architecture on these results. In previous work, we have shown that macroscopic properties in these networks are conserved for more local connectivity, as long as the the connexions remain sparse [El Boustani & Destexhe, 2009]. Therefore, the phase diagram for topological networks owns similar structures as those displayed in Fig. 7. However, in the limit of “first-neighbor” connectivity, correlations between neurons become

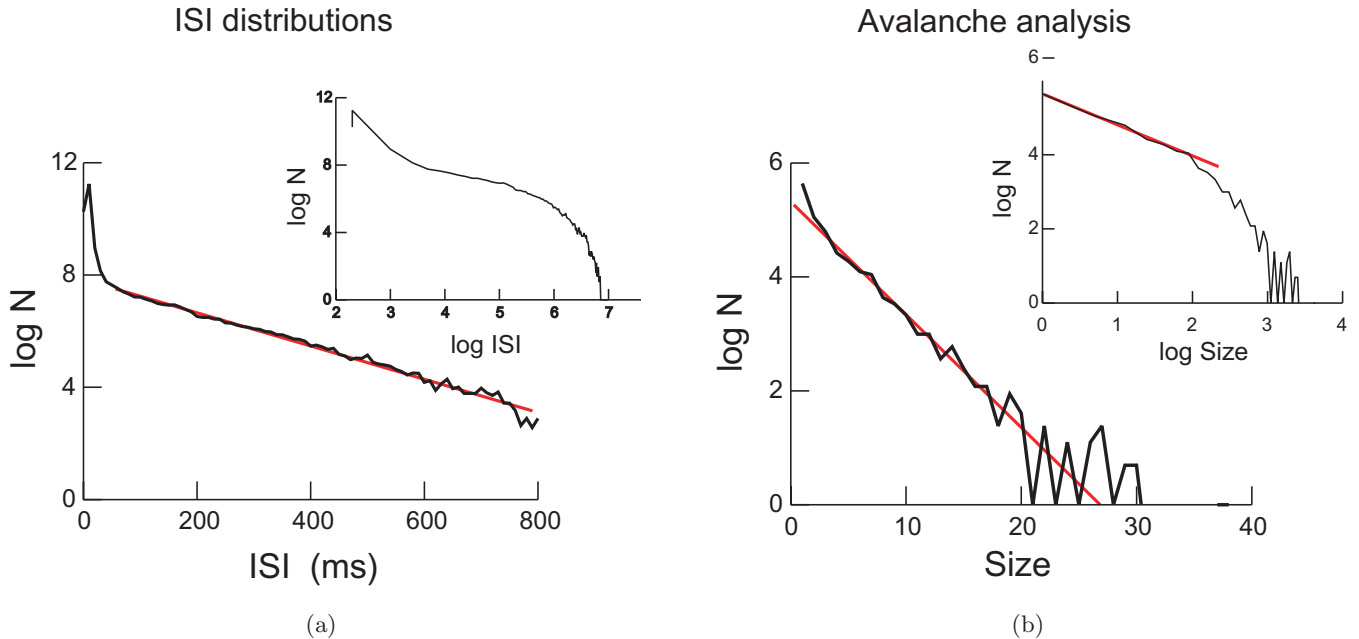


Fig. 10. Analysis of the network dynamics in a model of asynchronous irregular states. (a) ISI distributions during the AI state in a randomly-connected network of 16 000 integrate-and-fire neurons. ISI distributions are exponential (noisy trace), as predicted by a Poisson process (red line; inset: log–log representation using natural logarithms). (b) Absence of avalanche dynamics in this model (same description as Fig. 6(b)). The red lines indicate regions of exponential scaling; the red line in inset indicates a region with power-law scaling. Modified from [El Boustani *et al.*, 2007].

significantly stronger and the resulting neuronal dynamics are more regular and far from biological observations. Thus, even though more local architectures can result in more correlated activity, these correlations have to remain small in order to preserve the network stability and the rich repertoire of regimes. Our results are thus general for locally-connected networks as long as the sparseness is respected.

6. How to Reconcile these Data?

The above data show that in both human, cat and models, the dynamics can show clear signs of coherence and low dimensionality at the level of macroscopic measurements (EEG, LFPs, averages), while microscopically, neuronal dynamics are highly irregular and resemble stochastic processes. In an attempt to reconcile these observations, we rely on recently introduced generalization of classical nonlinear tools. In particular, Finite-Size Lyapunov Exponent [Aurell *et al.*, 1997; Shibata & Kaneko, 1998; Cencini *et al.*, 1999; Gao *et al.*, 2006] and the ϵ -entropy [Cencini *et al.*, 2000] have proven to be valuable measures to probe the system which displays different behaviors at different scales. In the present context, where low-dimensional dynamics

can take place on top of a highly irregular neuronal behavior, those measures appear as the most natural.

They were applied to the human EEG, as shown in Fig. 11. The FSLE in the upper panel neither possess a plateau nor behaves according to a power-law except in the small-scale limit where the stochastic-like component is dominant. For Creutzfeldt–Jacob disease as well as for epileptic seizure, however, it seems that a small region displays an almost scale-free behavior which would indicate a low-dimensional chaotic dynamics. Following [Shibata & Kaneko, 1998], it seems that the cortical activity exists in a high-dimensional attractor which could be chaotic. Therefore, the FSLE does not really help to untangle the different scales of dynamics here. However, when resorting to the ϵ -entropy, we get a different picture. Figure 11(b) clearly shows that most of these cortical states manifest a large plateau on large-scale. These plateau is a signature of low-dimensional dynamics [Cencini *et al.*, 2000] whereas the small-scale power-law behavior is the signature of stochastic-like dynamics produced by high-dimensional attractor. In accordance with Fig. 3, the dynamics during being eyes-open awake and REM sleep do not own a plateau, and their attractor dimension is too high to be distinguished

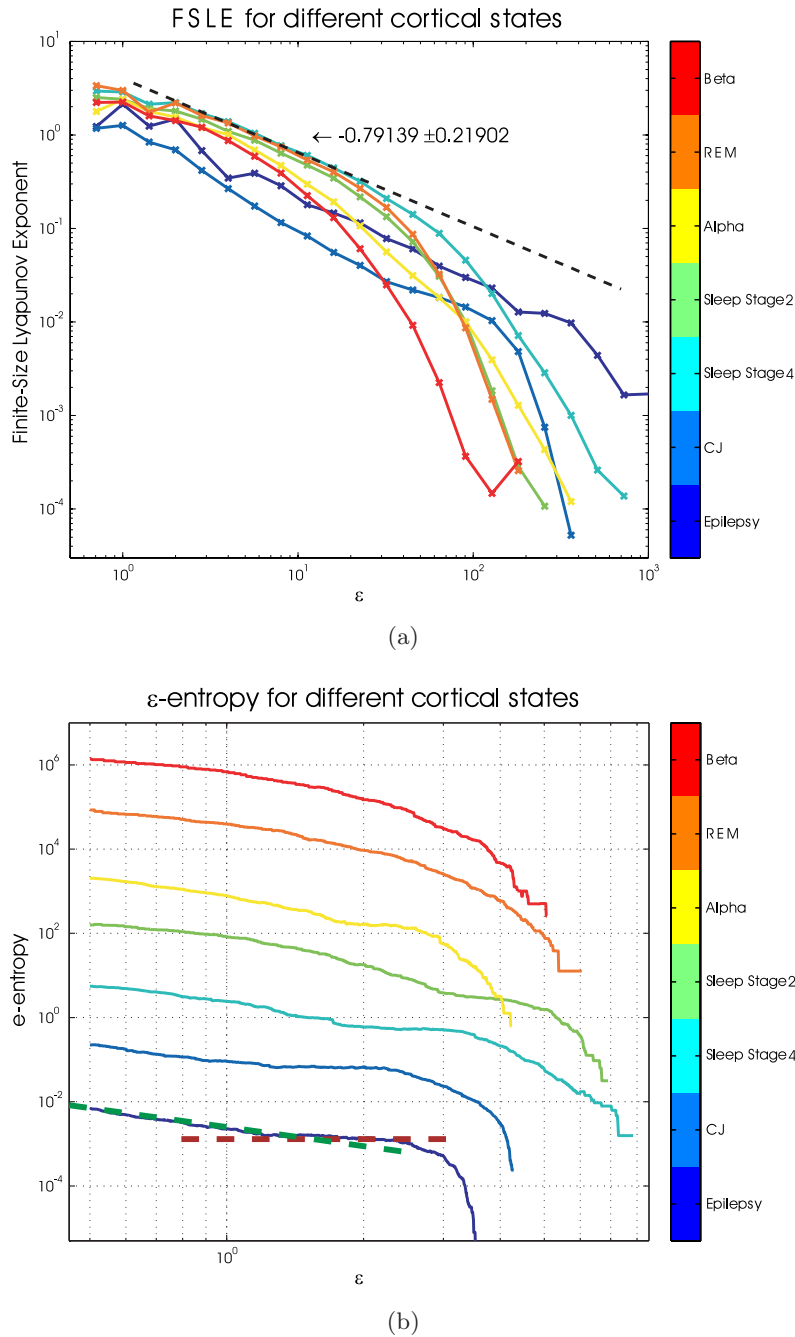


Fig. 11. Scale-dependent Lyapunov exponent and Epsilon-entropy for different brain states. The scale-dependent Lyapunov exponent (a) and ϵ -entropy (b) were calculated from the same EEG states as shown in Fig. 1. The FSLE (a) does not show any plateau and if the inverse FSLE is plotted in a semilog scale on the x -axis, no low-dimensional chaotic behavior can be detected for most states (data not shown). Following [Shibata & Kaneko, 1998] example for general coupled maps, the macroscopic activity seems to exhibit high-dimensional chaotic dynamics. For small scales $\epsilon \rightarrow 0$, a scale-free region is found with a power-law exponent around 0.791 (black dotted line) as expected from the microscopic stochastic-like dynamics [Cencini *et al.*, 2000; Gao *et al.*, 2006]. Because of the absence of a large scale-free region in the semilog region, we cannot define a macroscopic Lyapunov exponent from this measure. However, for the Creutzfeldt–Jacob disease and the epileptic seizure, the FSLE have a free-scale region on a broad range which is different from the other cortical states. This could indicate a low-dimensional chaotic dynamic even though it is not reflected in the semilog scale. Indeed, the ϵ -entropy (b) manifests a clear plateau (red dotted line) for the epileptic seizure, the Creutzfeldt–Jakob disease, sleep stages 2 and 4 and the alpha waves. This plateau indicates the existence of a low-dimensional attractor on the corresponding scales [Cencini *et al.*, 2000] which can sometimes be easily visualized with an embedding procedure (see Fig. 1). For REM and awake states, this plateau disappears leaving the dynamics in a stochastic-like (high-dimension) state at all scales. The small-scale behavior is identical to the FSLE (green dotted line).

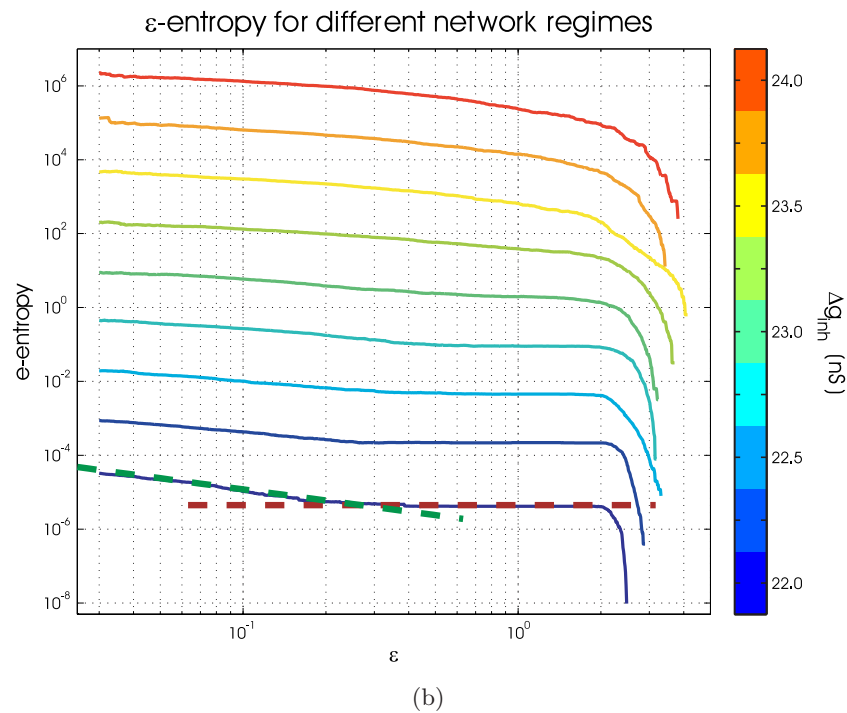
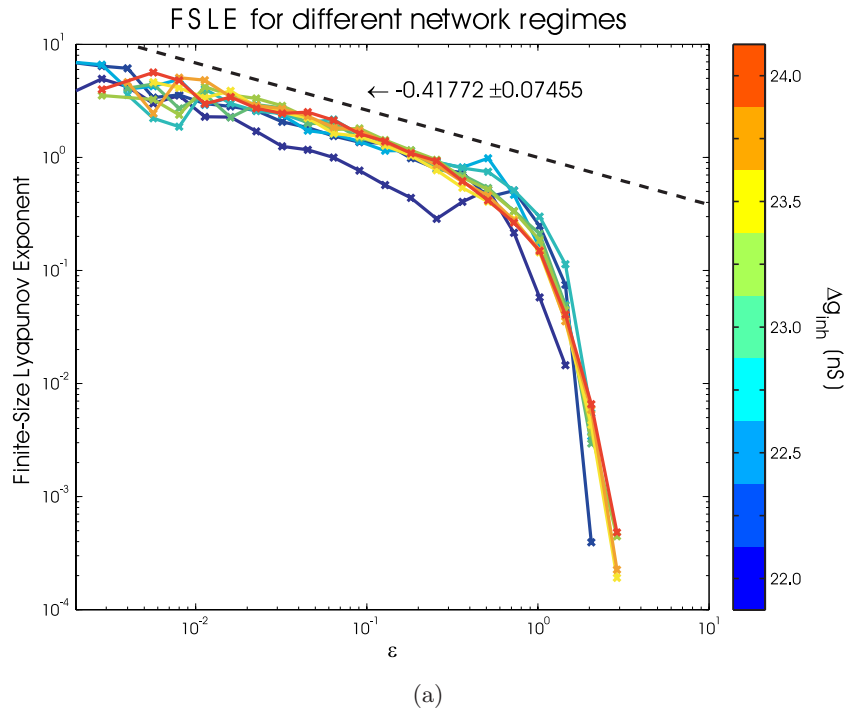


Fig. 12. Scale-dependent Lyapunov exponent and Epsilon-entropy for different network states. The Finite-Size Lyapunov Exponent (a) and ϵ -entropy (b) were calculated from the same network states as shown in Fig. 7. The FSLE behaves almost identically for every network state. There is no evidence for a low-dimensional chaotic dynamics which would be indicated by a scale-free region in intermediate scales. The power-law at small-scale owns a coefficient around 0.418 (black dotted line) characterizing the stochastic-like dynamic (high-dimensional deterministic) at those scales. Even though no evidence for low-dimension chaos can be found from the FSLE, the ϵ -entropy (b) has a large plateau (red dotted line) for state lying in the SR region (low inhibitory conductance). This plateau is shortened when the network dynamics is driven toward the AI regime where eventually the dynamics is indistinguishable from stochastic process. The small-scale behavior is identical to the FSLE (green dotted line).

from noise. However, it should be noted that those different dynamics are produced by the same system hence being mainly modulated by endogenic factors. In light of this result, we can conclude that there is no contradiction between the experimental data acquired at the macroscopic level (EEG) and that the microscopic level (Spiking Activity). For large network of coupled units, averaged quantities can display low-dimensional structured dynamics while being seemingly stochastic at a smaller scale.

We also evaluated the same quantities from the averaged activities of the numerical model. In Fig. 12(a), we see as before that the FSLE does not exhibit any scale-free region except for the small-scale limit. Thus we cannot rely on this measure to distinguish small- and large-scale behaviors. In contrast, the ϵ -entropy in Fig. 12(b) yields a large and distinct plateau in the SR regime. The disappearance of this plateau has been used as a criteria to draw the dotted black line in Fig. 9. For inhibitory conductances larger than $\Delta g_{\text{inh}} \simeq 23.5$ (nS), the ϵ -entropy slowly converges to its small-scale stochastic-like behavior. We thus recover a very comparable behavior to the EEG data where pathological states or deep sleep produce structured activity at the EEG level and awake state or REM are comparable to the dynamics of AI regime, as suggested previously [van Vreeswijk & Sompolinsky, 2006; 2008; Vogels & Abbott, 2005; El Boustani *et al.*, 2007; Kumar *et al.*, 2008].

7. Discussion

In this paper, we have briefly reviewed correlation dimension analyses of human EEG, which revealed a hierarchy of brain states, where the dimensionality varies approximately inversely to the level of arousal (Fig. 4). In particular, awake and attentive subjects display high dimensionalities, while deep sleep of pathological states show evidence for low dimensionalities. These low dimensions are difficult to reconcile with the fact that these signals emanate from the activity of millions (if not billions) of neurons. In cat cerebral cortex, the cellular activity during wake and sleep are highly irregular, and exponentially distributed like stochastic (Poisson) processes, a feature which is also difficult to reconcile with low dimensionalities at the EEG level, even though LFP data do not manifest low-dimensional dynamics (data not shown). We performed similar analyses on computational models, which also

display these apparently coherent activities at the level of large-scale averages, while the microscopic activity is highly irregular. In particular, SR states can display coherent behavior at large scales, while AI states do not show evidence for coherence, similar to recordings in awake cats and humans.

The nature of the dynamics exhibited by models is assimilable to high-dimensional chaos. It has been shown that AI states in such models shut down after some time, and are thus transient in nature [Vogels & Abbott, 2005; El Boustani *et al.*, 2007; Kumar *et al.*, 2008; El Boustani & Destexhe, 2009]. This lifetime has been estimated to increase exponentially with the network size [Kumar *et al.*, 2008; El Boustani & Destexhe, 2009], and can reach considerable times (beyond any reasonable simulation time; [Kumar *et al.*, 2008]). Moreover, other recent studies [Cessac, 2008; Cessac & Viéville, 2008] have obtained analytical results on similar models where “transient chaotic-like regimes” were found. More precisely, these regimes are periodic, but with a period which also grows exponentially with network size. These results are reminiscent of the nonattractive chaotic manifolds extensively discussed in the literature [Crutchfield & Kaneko, 1988; Dhamala *et al.*, 2001; Dhamala & Lai, 2002; Tél & Lai, 2008; Zillmer *et al.*, 2006]. Hence, even though the chaotic nature of the dynamics is not inherent of the underlying system, the network spends a long enough period trapped in this transient dynamics indistinguishable from chaos from a numerical point of view.

To characterize the dynamics at different scales, we estimated quantities such as FSLE or ϵ -entropy, which clearly show that microscopic scales (neurons) tend to be very high-dimensional and complex, in many ways similar to “noise”, while more coherent behavior can be present at large scales. This analysis is consistent with the recently proposed concept of “macroscopic chaos”, where a very high-dimensional microscopic dynamics coexists with low dimensionality at the macroscopic level. In this paper, the chosen numerical model is known to be purely deterministic and can display highly irregular spiking patterns close to stochastic processes or noise. From a nonlinear analysis point of view, most of this dynamics is indistinguishable from a random process. However, as soon as a large scale behavior emerge, the ϵ -entropy can keep track of it and still manifest the small-scale irregular fluctuations.

We conclude that numerical models of recurrent neuronal networks, with conductance-based

integrate-and-fire neurons, can be assimilated to high-dimensional chaotic systems, and are in many ways similar to the EEG. Moreover, even though they exhibit limit-cycle regimes for several parameter sets, this collective dynamics is built on top of irregular and high-dimensional neuronal activity which is only apparent at small-scales. Interestingly, this scheme reminds of fluid dynamics, where a seemingly random microscopic dynamics may also coexist with more coherent behavior at large scales. This is the case, for example, close to the transition to turbulence, where fluids can show evidence for low-dimensional chaos [Brandstater *et al.*, 1983]. More developed turbulence, however, does not show such evidence, presumably because a large number of degrees of freedom have been excited and the high-dimensional dynamics is present at all scales. It is possible that similar considerations apply to brain dynamics, especially when considering the recent debate about the nature of the ongoing activity of visual primary cortex (V1). Recordings made using voltage-sensitive dyes imaging (VSDI) in this cortical area have suggested that spontaneous activity consists of a seemingly-random replay of sensory-evoked orientation maps of activity in anesthetized [Kenet *et al.*, 2003], but not in awake animals [Omer *et al.*, 2008]. These observations have raised the question of whether the cortical activity of V1 could be described by a single-state high-dimensional attractor or a low-dimensional multistable attractor [Goldberg *et al.*, 2004]. It is likely that at the VSDI scale, both scenarios are possible at the same time but at different scales, which would be consistent with the present results.

Acknowledgments

Research supported by the CNRS, ANR and the European Community (FACETS grant FP6 15879). More details are available at <http://cns.iaf.cnrs-gif.fr>

References

- Albers, D. J., Sprott, J. C. & Crutchfield, J. P. [2006] “Persistent chaos in high dimensions,” *Phys. Rev. E* **74**, 057201.
- Aurell, E., Boffetta, G., Crisanti, A., Paladin, G. & Vulpiani, A. [1997] “Predictability in the large: An extension of the concept of Lyapunov exponent,” *J. Phys. A* **30**, 1–26.
- Babloyantz, A. & Destexhe, A. [1986] “Low dimensional chaos in an instance of epileptic seizure,” *Proc. Natl. Acad. Sci. USA* **83**, 3513–3517.
- Babloyantz, A., Nicolis, C. & Salazar, M. [1985] “Evidence for chaotic dynamics of brain activity during the sleep cycle,” *Phys. Lett. A* **111**, 152–156.
- Bédard, C., Kröger, H. & Destexhe, A. [2006] “Does the 1/f frequency scaling of brain signals reflect self-organized critical states?” *Phys. Rev. Lett.* **97**, 118102.
- Beggs, J. & Plenz, D. [2003] “Neuronal avalanches in neocortical circuits,” *J. Neurosci.* **23**, 11167–11177.
- Bertschinger, N. & Natschläger, T. [2004] “Real-time computation at the edge of chaos in recurrent neural networks,” *Neural Comp.* **16**, 1413–1436.
- Brandstater, A., Swift, J., Swinney, H. L., Wolf, A., Farmer, J. D., Jen, E. & Crutchfield, J. P. [1983] “Low-dimensional chaos in a hydrodynamic system,” *Phys. Rev. Lett.* **51**, 1442–1445.
- Cencini, M., Falcioni, M., Vergni, D. & Vulpiani, A. [1999] “Macroscopic chaos in globally coupled maps,” *Physica D* **130**, 58–72.
- Cencini, M., Falcioni, M., Olbrich, E., Kantz, H. & Vulpiani, A. [2000] “Chaos or noise: Difficulties of a distinction,” *Physica D* **130**, 58–72.
- Cessac, B. [2008] “A discrete time neural network model with spiking neurons; Rigorous results on the spontaneous dynamics,” *J. Math. Biol.* **56**, 311–345.
- Cessac, B. & Viéville, T. [2008] “On dynamics of integrate-and-fire neural networks with conductance based synapses,” *Front. Comput. Neurosci.* **2**.
- Crutchfield, J. P. & Kaneko, K. [1988] “Are attractors relevant to turbulence?” *Phys. Rev. Lett.* **60**, 2715–2718.
- Destexhe, A., Sepulchre, J. A. & Babloyantz, A. [1988] “A comparative study of the experimental quantification of deterministic chaos,” *Phys. Lett. A* **132**, 101–106.
- Destexhe, A. [1992] *Nonlinear Dynamics of the Rhythmical Activity of the Brain* (in French), Doctoral Dissertation (Université Libre de Bruxelles, Brussels, 1992). http://cns.iaf.cnrs-gif.fr/alain_thesis.html.
- Destexhe, A., Contreras, D. & Steriade, M. [1999] “Spatiotemporal analysis of local field potentials and unit discharges in cat cerebral cortex during natural wake and sleep states,” *J. Neurosci.* **19**, 4595–4608.
- Dhamala, M., Lai, Y.-C. & Holt, R. D. [2001] “How often are chaotic transients in spatially extended ecological systems?” *Phys. Lett. A* **280**, 297–302.
- Dhamala, M. & Lai, Y.-C. [2002] “The natural measure of nonattracting chaotic sets and its representation by unstable periodic orbits,” *Int. J. Bifurcation and Chaos* **12**, 2991–3005.
- Eckmann, J. P., Kamphorst, S. O. & Ruelle, D. [1987] “Recurrence plots of dynamical systems,” *Europhys. Lett.* **5**, 973–977.

- Elbert, T., Ray, W. J., Kowalik, Z. J., Skinner, J. E., Graf, K. E. & Birbaumer, N. [1994] "Chaos and physiology: Deterministic chaos in excitable cell assemblies," *Physiol. Rev.* **74**, 1–47.
- El Boustani, S., Pospischil, M., Rudolph-Lilith, M. & Destexhe, A. [2007] "Activated cortical states: Experiments, analyses and models," *J. Physiol. Paris* **101**, 99–109.
- El Boustani, S. & Destexhe, A. [2009] "A master equation formalism for macroscopic modeling of asynchronous irregular activity states," *Neural Comp.* **21**, 46–100.
- Frank, G. W., Lookman, T., Nerenberg, M. A. H., Essex, C. & Lemieux, J. [1990] "Chaotic time series analysis of epileptic seizures," *Physica D* **46**, 427–438.
- Fraser, A. M. & Swinney, H. L. [1986] "Independent coordinates for strange attractors from mutual information," *Phys. Rev. A* **33**, 1134–1140.
- Gao, J. B., Hu, J., Tung, W. W. & Cao, Y. H. [2006] "Distinguishing chaos from noise by scale-dependent Lyapunov exponent," *Phys. Rev. E* **74**, 066204.
- Gaspard, P. & Wang, X. J. [1993] "Noise, chaos, and (τ, ϵ) -entropy per unit time," *Phys. Rep.* **235**, 321–373.
- Goldberg, J. A., Rokni, U. & Sompolinsky, H. [2004] "Patterns of ongoing activity and the functional architecture of the primary visual cortex," *Neuron* **42**, 489–500.
- Grassberger, P. & Procaccia, I. [1983] "Measuring the strangeness of strange attractors," *Physica D* **9**, 189208.
- Hegger, R., Kantz, H. & Schreiber, T. [1999] "Practical implementation of nonlinear time series methods: The TISEAN package," *Chaos* **9**, 413–435.
- Jensen, H. J. [1998] *Self-Organized Criticality. Emergent Complex Behavior in Physical and Biological Systems* (Cambridge University Press, Cambridge UK).
- Kantz, H. & Shreiber, T. [2004] *Nonlinear Time Series Analysis* (Cambridge University Press).
- Kenet, T., Bibitchkov, D., Tsodyks, M., Grinvald, A. & Arieli, A. [2003] "Spontaneously emerging cortical representations of visual attributes," *Nature* **425**, 954–956.
- Korn, H. & Faure, P. [2003] "Is there chaos in the brain? II. Experimental evidence and related models," *C.R. Biol.* **326**, 787–840.
- Kumar, A., Schrader, S., Aertsen, A. & Rotter, S. [2008] "The high-conductance state of cortical networks," *Neural Comput.* **20**, 1–43.
- Legenstein, R. & Maass, W. [2007] "Edge of chaos and prediction of computational performance for neural circuit models," *Neural Net.* **20**, 323–334.
- Marwan, N., Romano, M. C., Thiel, M. & Kurths, J. [2006] "Recurrence plots for the analysis of complex systems," *Phys. Rep.* **438**, 237–329.
- Mayer-Kress, G., Yates, F. E., Benton, L., Keidel, M., Tirsh, W., Poppl, S. J. & Geist, K. [1988] "Dimension analysis of nonlinear oscillations in brain, heart and muscle," *Math. Biosci.* **90**, 155–182.
- Sauer, T., Yorke, J. A. & Casdagli, M. [1991] "Embedology," *J. Stat. Phys.* **65**, 579–616.
- Shibata, T. & Kaneko, K. [1998] "Collective chaos," *Phys. Rev. Lett.* **81**, 4116.
- Sompolinsky, H., Crisanti, A. & Sommers, H. J. [1988] "Chaos in random neural networks," *Phys. Rev. Lett.* **61**, 259–262.
- Sprott, J. C. [2008] "Chaotic dynamics on large networks," *Chaos* **18**, 023135.
- Takens, F. [1981] "Detecting strange attractors in turbulence," *Dynamical Systems and Turbulence*, Lecture Notes in Mathematics, Vol. 898 (Springer, Berlin).
- Tél, T. & Lai, Y.-C. [2008] "Chaotic transients in spatially extended systems," *Phys. Rep.* **460**, 245–275.
- Theiler, J. [1990] "Estimating fractal dimension," *J. Opt. Soc. Amer. A* **7**, 1055.
- van Vreeswijk, C. A. & Sompolinsky, H. [1996] "Chaos in neuronal networks with balanced excitatory and inhibitory activity," *Science* **274**, 1724–1726.
- van Vreeswijk, C. A. & Sompolinsky, H. [1998] "Chaotic balanced state in a model of cortical circuits," *Neural Comp.* **10**, 1321–1372.
- Vogels, T. P. & Abbott, L. F. [2005] "Signal propagation and logic gating in networks of integrate-and-fire neurons," *J. Neurosci.* **25**, 10786–10795.
- Wolf, A., Swift, J. B., Swinney, H. L. & Vastano, J. A. [1985] "Determining Lyapunov exponents from a time series," *Physica D* **16**, 285–317.
- Zillmer, R., Livi, R., Politi, A. & Torcini, A. [2006] "Desynchronization in diluted neural networks," *Phys. Rev. E* **74**, 036203.